

Origin of Oxygen Partial Pressure-Dependent Conductivity in SrTiO₃

Zenghua Cai^{1,2,a)} and Chunlan Ma^{1,2}

¹Key Laboratory of Intelligent Optoelectronic Devices and Chips of Jiangsu Higher Education Institutions, School of Physical Science and Technology, Suzhou University of Science and Technology, Suzhou, 215009, China

²Advanced Technology Research Institute of Taihu Photon Center, School of Physical Science and Technology, Suzhou University of Science and Technology, Suzhou, 215009, China

^{a)}**Authors to whom correspondence should be addressed:** zhcai@usts.edu.cn

Abstract

SrTiO₃ (STO) displays a broad spectrum of physical properties, including superconductivity, ferroelectricity, and photoconductivity, making it a standout semiconductor material. Despite extensive researches, the oxygen partial pressure-dependent conductivity in STO has remained elusive. This study leverages first-principles calculations, and systematically investigates the intrinsic defect properties of STO. The results reveal that V_O, V_{Sr}, and Ti_{Sr} are the dominant intrinsic defects, influencing STO's conductivity under varying O chemical potentials (oxygen partial pressures). Under O-poor condition, V_O is the predominant donor, while V_{Sr} is the main acceptor. As the oxygen pressure increases, Ti_{Sr} emerges as a critical donor defect under O-rich condition, significantly affecting the conductivity. Additionally, the study elucidates the abnormal phenomenon where V_{Ti}, typically an acceptor, exhibits donor-like behavior due to the formation of O-trimer. This work offers a comprehensive understanding of how intrinsic defects tune the Fermi level, thereby altering STO's conductivity from metallic to n-type, and eventually to p-type across different O chemical potentials. These insights resolve the long-standing issue of oxygen partial pressure-dependent conductivity and explain the observed metallic conductivity in oxygen-deficient STO.

As a prototypical perovskite, SrTiO₃ (STO) possesses many fascinating physical properties such as superconductivity¹, ferroelectricity²⁻⁴, photoconductivity⁵, two-dimensional (2D) electron gas⁶, blue-light emission⁷, magnetic effect⁸, thermoelectric coefficient⁹, metal-insulator transition¹⁰, spin-charge conversion¹¹, and spin splitting¹². Recently, two new physical properties have also been reported, i.e., terahertz electric-field-driven dynamical multiferroicity¹³ and highly reversible extrinsic electrocaloric effect¹⁴. With all these attractive properties, STO has become a unique semiconductor which has received much attention in recent decades.

Point defects are of special importance to semiconductors. As a unique semiconductor, the defect properties of STO are undoubtedly important and have been intensively studied. In experiment, studies on the defect properties of STO can mainly be divided into two aspects: (i) focusing on the defect itself, such as the identification of cation vacancies (V_{Ti} and V_{Sr})¹⁵, direct observation of Sr vacancy (V_{Sr})¹⁶, discovering the abundant Ti_{Sr} antisite¹⁷, and confirming the existence of Ti vacancy (V_{Ti})¹⁸; (ii) the effects induced by the defect, such as high electron mobility induced by the V_{Sr} clusters¹⁹, photo-activated electron transport governed by defect complexes²⁰, photoconductivity related to V_{Sr} ²¹, and photoflexoelectricity enhanced by the oxygen vacancy (V_{O})²². Similarly, theoretical investigations of defects in STO can also be classified into the same two aspects. For the defect itself, the studies includes intrinsic defects²³⁻²⁸, impurity defects²⁹⁻³², and different methods for simulating defect properties in STO³³⁻³⁷. For the defect correlated effects, studies include the coloration in Fe-doped STO³⁸, high temperature conductivity influenced by impurity defects³⁹, persistent photoconductivity caused by substitutional hydrogen (H_{O})⁴⁰, ferroelectricity and blue light emission related to Ti antisite defect (Ti_{Sr})⁴¹, and so on⁴²⁻⁴⁵.

Even though so much effort has been made, a long-standing issue correlated with defects, i.e., the origin of oxygen partial pressure-dependent conductivity, still remains unsolved. As early as 1995, Akhtar et al. has pointed out this issue⁴⁶. As the increase of the oxygen partial pressure, the conductivity of STO first decreases and then increases. Meanwhile, the type of conductivity changes from n-type to p-type. In 2003, Tanaka et al. explained this issue from the perspective of intrinsic vacancies based on local density approximation (LDA)⁴⁷. More recently, Wu et al. performed a grand canonical multiscale simulation and analyzed this issue from the perspective of grain size⁴⁸. As is well known, the conductivity of a semiconductor (without doping) is mainly determined by the intrinsic point defects, including vacancy, antisite and interstitial. However, a systematic study on the oxygen partial pressure-dependent conductivity

in STO from the perspective of intrinsic point defects is still lacking. Hence, we performed a systematic first-principles study on the intrinsic point defect properties of STO in this work.

Defect properties are mainly determined by the structures of defects. In order to predict the defect properties precisely, it is necessary to locate the ground-state structures accurately. Therefore, we used the ShakeNBreak to find out the ground-state structures of defects in this work⁴⁹. Since it is very time-consuming to relax different distorted defect structures, the bond distortions are only considered for neutral defects. For example, Fig. 1(a) shows the final total energies of neutral V_O versus bond distortion factor (see supplementary materials for computational details). As we can see, 9 distorted structures are considered for neutral V_O . Most of the distorted structures have the similar total energies around -1069 eV after relaxation (for 135-atom supercell). Only one structure has a relatively high total energy around -1062 eV, which is confirmed unreasonable after checking the relaxed structure. Among the remaining 8 distorted structures, they all have similar configurations after relaxation as shown in Fig. 1(b). Two Ti atoms (adjacent to V_O) move slightly away from the position of V_O , consistent with the previous reports^{25,36}. The final ground-state structure for neutral V_O is taken as the one without initial distortions, marked with a red star in Fig. 1(a), since this structure has the lowest total energy. Moreover, for the charged defects, their initial structures (before relaxation) come from the related neutral ground-state structures identified by ShakeNBreak.

In order to find out the dominant intrinsic defects affecting the conductivity, the formation energies of all the non-equivalent intrinsic defects are calculated, including vacancies (V_{Sr} , V_{Ti} , V_O), antisites (Sr_{Ti} , Sr_O , Ti_{Sr} , Ti_O , O_{Sr} , O_{Ti}) and interstitials. For the interstitials, five random non-equivalent interstitial sites are considered for Sr, Ti and O atoms. Then, the lowest energy configuration is picked as the candidate. For example, the second interstitial site for Sr (Sr_{i2}) is the most stable, hence Sr_{i2} is selected as the candidate for Sr interstitial. For Ti and O atoms, Ti_{i3} and O_{i1} are chosen to represent the Ti and O interstitials, respectively. Fig. 2 shows the calculated formation energies as function of Fermi level (E_F) under different O chemical potentials (see supplementary materials for the selection of chemical potential). Under O-poor condition (low oxygen partial pressure), the dominant donor defect is V_O and it is always in +2 charge state. This means there is no defect transition level for V_O in the band gap as shown in Fig. 3(d). Meanwhile, the dominant acceptor defect is V_{Sr} . It has a very shallow transition level from -1 to -2 charge state, and this level is 0.05 eV above the valence band maximum (VBM). Moreover, the donor defects Ti_{Sr} , Ti_{i3} , Ti_O and Sr_O also have relatively low formation energies, while according to the analysis of defect densities as shown in Fig. 4, the densities of these

donor defects are relatively low. Hence, their influence on the conductivity is limited, and they are not the dominant donor defects under O-poor condition.

As the oxygen partial pressure increases, the chemical potential of O will change to mediate condition. In this situation, the prominent donor and acceptor defects are still V_O and V_{Sr} as shown in Fig. 2(b). As the oxygen partial pressure increases further, the chemical potential of O will become rich. At this moment, the dominant acceptor defect is still V_{Sr} , while the dominant donor defects become V_O and Ti_{Sr} . Although the formation energy of Ti_{Sr} has an upward trend with the increase of the O chemical potential, its contribution to conductivity increases abnormally. The reason behind this is that as the O chemical potential increases, the Fermi level decreases, and the defect density of donor Ti_{Sr} increases as shown in Fig. 4. Especially for +2 charge state Ti_{Sr} , its density can go beyond 10^{19} cm^{-3} . Therefore, Ti_{Sr} is the dominant donor defect under O-rich condition. For Ti_{Sr} , it also has a very shallow transition level from +2 to +1 charge state, and it is 0.1 eV below the conduction band minimum (CBM) as shown in Fig. 3(d). In addition, the donor defect O_{i1} also has a relatively low formation energy 0.65 eV for the neutral state, and it has two deep transition levels in the band gap as shown in Fig. 3(d). The first one is from +1 to neutral state (2.85 eV below the CBM), and the second one is from +3 to +1 charge state (3.08 eV below the CBM). These two deep transition levels may serve as carrier trap levels or even recombination centers. Fortunately, the influence of O_{i1} on the conductivity should be small compared with V_O and Ti_{Sr} , since it is neutral in most cases when E_F changes in the range of the band gap.

Based on the above discussion, we can determine that the main intrinsic defects are V_O , V_{Sr} and Ti_{Sr} . This explains why many researchers focus on the vacancies (especially V_O) and Ti_{Sr} ^{16,17,25,27,35,36,47,50}. Among all the intrinsic defects, an abnormal phenomenon is observed for V_{Ti} , which has a relatively low formation energy under O-rich condition as shown in Fig. 2(c). As we all know, cation vacancy is usually an acceptor, while V_{Ti} is a donor based on our results. In fact, this can be understood after analyzing the defect structure of V_{Ti} . As shown in Fig. 3(a), after removing a Ti atom (forming V_{Ti}), the O atom (yellow ball) above the removed Ti will break its bond with the Ti atom above it and then move downward, forming an O-trimer. To understand this process clearly, it is illustrated using a planar figure. As shown in Fig. 3(b), one Ti atom (+4 charge state in STO) will bond with four O atoms, forming four single bonds. After removing the left Ti atom as shown in Fig. 3(b), one V_{Ti} and four O dangling bonds will be formed. Usually, four O dangling bonds need four electrons to achieve the full-shell stable state. Hence, V_{Ti} should accept the electron and be an acceptor. However, in STO as shown in Fig.

3(c), the middle O atom (yellow ball) will break its bond with the right Ti atom and form an O-trimer with the left two O atoms. In this situation, the previous four O dangling bonds will change to one O dangling bond and one Ti dangling bond, leaving two unpaired electrons as shown in Fig. 3(c). The unpaired electron of O atom tends to accept one electron, while the unpaired electron of Ti atom tends to donate one electron. Therefore, V_{Ti} could be acceptor, donor or even both. After checking the calculation results, only two single-occupied states (considering the spin polarization) are found in the band gap of STO, and thus V_{Ti} is a donor. For V_{Ti} , it has a relatively high formation energy compared with V_O and V_{Sr} (This is consistent with the results reported by Janotti et al.²⁵), and hence its influence on the conductivity of STO should be limited.

Fig. 3(d) shows the transition levels of all the intrinsic defects in STO. As we can see, the dominant intrinsic defects either have no transition level in the band gap (like V_O), or have very shallow transition levels (like V_{Sr} and Ti_{Sr}). This means these defects will never act as the trap states. For the rest intrinsic defects, even though some of them (Sr_{Ti2} , Ti_{i3} , Sr_{Ti} , O_{Ti} and V_{Ti}) have deep transition levels as shown in Fig. 3(d), their influence on the intrinsic carriers and conductivity of STO should be limited, since their formation energies are high, which means their defect densities are low. Meanwhile, most of the intrinsic defects are donor defects. The donor will donate electrons and push up the Fermi level. This could be one of the factors contributing to the unintentional n-type conductivity of STO.

At last, to unravel the origin of oxygen partial pressure-dependent conductivity quantitatively, the density of low-energy intrinsic defects, Fermi level (E_F) and intrinsic carrier densities in STO as function of O chemical potential (oxygen partial pressure) are calculated as shown in Fig. 4. Based on the results of E_F , the range of O chemical potential can be classified into three typical regions. The first region (R1) is where the E_F is located above the band gap (E_g). In this region, E_F goes beyond the CBM and STO shows metallic conductivity when the O chemical potential is poor (oxygen partial pressure is low). At this moment, the density of intrinsic electron carrier is extremely high, close to 10^{20} cm^{-3} . The dominant intrinsic defects are V_O^{1+} , V_O^{2+} and V_{Sr}^{2-} , and the density of V_O^{1+} can go beyond that of V_O^{2+} , which can not be directly discovered from the formation energy results as shown in Fig. 2. Moreover, the density of V_O^0 can be higher than 10^{23} cm^{-3} , indicating that STO should be oxygen-deficient under this condition. Intriguingly, the metallic conductivity was reported long ago in oxygen-deficient STO under low oxygen partial pressure⁵¹. This validates the robustness of our results.

As the increase of oxygen partial pressure, the O chemical potential enters the second region (R2). In this region, STO can show excellent n-type conductivity. In this situation, E_F is very close to CBM (0-0.29 eV below the CBM) and the intrinsic electron carrier density is high (10^{14} - 10^{19} cm⁻³). At this moment, the donor V_O^{2+} , V_O^{1+} , Ti_{Sr}^{2+} , Ti_{Sr}^{1+} and acceptor V_{Sr}^{2-} are the dominant intrinsic defects affecting the conductivity. Their defect densities are all higher than 10^{15} cm⁻³. For the third region (R3), the oxygen partial pressure is very high (O chemical potential is very rich). In this region, the conductivity of STO goes through a transition from n-type to p-type. This can be deduced from the change of the E_F from above the middle of the band gap ($E_g/2$) to below the middle of band gap (about 0.5 eV above the VBM). Meanwhile, the intrinsic carrier changes from electron to hole, and its density is about 10^{11} cm⁻³. In this region, STO shows benign p-type conductivity, which is also observed in experiment^{52,53}. Furthermore, O_{i1}^{1+} is also an important intrinsic defect in addition to the Ti_{Sr}^{2+} , V_O^{2+} and V_{Sr}^{2-} under this condition. Its density is about 10^{15} - 10^{17} cm⁻³.

In summary, the intrinsic defect properties have been systematically studied based on the first-principles calculations. The results show that the dominant intrinsic defects are V_O , V_{Sr} and Ti_{Sr} . As the change of the O chemical potential, these dominant intrinsic defects can tune the Fermi level from above the middle of the band gap to below the middle of the band gap. Hence, STO can exhibit metallic, excellent n-type and benign p-type conductivity under different O chemical potentials. These findings unravel the origin of the oxygen partial pressure-dependent conductivity from the perspective of intrinsic point defects. Furthermore, our results also uncover the microscopic mechanism behind the experimentally discovered metallic conductivity in oxygen-deficient STO.

SUPPLEMENTARY MATERIALS

See the supplementary materials to access the additional details of this work.

ACKNOWLEDGMENT

This work was supported by National Natural Science Foundation of China under grant No. 12304110.

DATA AVAILABILITY

The data that support the findings of this study are available from the corresponding author upon reasonable request.

REFERENCES

- ¹J. F. Schooley, W. R. Hosler, and M. L. Cohen, Superconductivity in Semiconducting SrTiO₃. *Phys. Rev. Lett.* **12**, 474 (1964).
- ²J. H. Haeni, P. Irvin, W. Chang, R. Uecker, P. Reiche, Y. L. Li, S. Choudhury, W. Tian, M. E. Hawley, B. Craigo, A. K. Tagantsev, X. Q. Pan, S. K. Streiffer, L. Q. Chen, S. W. Kirchoefer, J. Levy, and D. G. Schlom, Room-temperature ferroelectricity in strained SrTiO₃. *Nature* **430**, 758 (2004).
- ³H. W. Jang, A. Kumar, S. Denev, M. D. Biegalski, P. Maksymovych, C. W. Bark, C. T. Nelson, C. M. Folkman, S. H. Baek, N. Balke, C. M. Brooks, D. A. Tenne, D. G. Schlom, L. Q. Chen, X. Q. Pan, S. V. Kalinin, V. Gopalan, and C. B. Eom, Ferroelectricity in Strain-Free SrTiO₃ Thin Films. *Phys. Rev. Lett.* **104**, 197601 (2010).
- ⁴H. L. D. Lee, Y. Gu, S.-Y. Choi, S.-D. Li, S. Ryu, T. R. Paudel, K. Song, E. Mikheev, S. Lee, S. Stemmer, D. A. Tenne, S. H. Oh, E. Y. Tsymbal, X. Wu, L.-Q. Chen, A. Gruverman, C. B. Eom, Emergence of room-temperature ferroelectricity at reduced dimensions. *Science* **349**, 1314 (2015).
- ⁵M. C. Tarun, F. A. Selim, and M. D. McCluskey, Persistent photoconductivity in strontium titanate. *Phys. Rev. Lett.* **111**, 187403 (2013).
- ⁶A. Ohtomo and H. Y. Hwang, A high-mobility electron gas at the LaAlO₃/SrTiO₃ heterointerface. *Nature* **427**, 423 (2004).
- ⁷D. Kan, T. Terashima, R. Kanda, A. Masuno, K. Tanaka, S. Chu, H. Kan, A. Ishizumi, Y. Kanemitsu, Y. Shimakawa, and M. Takano, Blue-light emission at room temperature from Ar⁺-irradiated SrTiO₃. *Nat. Mater.* **4**, 816 (2005).
- ⁸A. Brinkman, M. Huijben, M. van Zalk, J. Huijben, U. Zeitler, J. C. Maan, W. G. van der Wiel, G. Rijnders, D. H. A. Blank, and H. Hilgenkamp, Magnetic effects at the interface between non-magnetic oxides. *Nat. Mater.* **6**, 493 (2007).
- ⁹H. Ohta, S. Kim, Y. Mune, T. Mizoguchi, K. Nomura, S. Ohta, T. Nomura, Y. Nakanishi, Y. Ikuhara, M. Hirano, H. Hosono, and K. Koumoto, Giant thermoelectric Seebeck coefficient of a two-dimensional electron gas in SrTiO₃. *Nat. Mater.* **6**, 129 (2007).
- ¹⁰Y. Lee, C. Clement, J. Hellerstedt, J. Kinney, L. Kinnischtzke, X. Leng, S. D. Snyder, and A. M. Goldman, Phase Diagram of Electrostatically Doped SrTiO₃. *Phys. Rev. Lett.* **106**, 136809 (2011).
- ¹¹P. Noël, F. Trier, L. M. Vicente Arche, J. Bréhin, D. C. Vaz, V. Garcia, S. Fusil, A. Barthélémy, L. Vila, M. Bibes, and J.-P. Attané, Non-volatile electric control of spin-charge conversion in a SrTiO₃ Rashba system. *Nature* **580**, 483 (2020).
- ¹²A. F. Santander-Syro, F. Fortuna, C. Bareille, T. C. Rödel, G. Landolt, N. C. Plumb, J. H. Dil, and M. Radović, Giant spin splitting of the two-dimensional electron gas at the surface of SrTiO₃. *Nat. Mater.* **13**, 1085 (2014).
- ¹³M. Basini, M. Pancaldi, B. Wehinger, M. Udina, V. Unikandanunni, T. Tadano, M. C. Hoffmann, A. V. Balatsky, and S. Bonetti, Terahertz electric-field-driven dynamical multiferroicity in SrTiO₃. *Nature* **628**, 534 (2024).
- ¹⁴S. Zhang, J. Deliyore-Ramírez, S. Deng, B. Nair, D. Pesquera, Q. Jing, M. E. Vickers, S. Crossley, M. Ghidini, G. G. Guzmán-Verri, X. Moya, and N. D. Mathur, Highly reversible

extrinsic electrocaloric effects over a wide temperature range in epitaxially strained SrTiO₃ films. *Nat. Mater.* **23**, 639 (2024).

¹⁵D. J. Keeble, S. Wicklein, R. Dittmann, L. Ravelli, R. A. Mackie, and W. Egger, Identification of A- and B-site cation vacancy defects in perovskite oxide thin films. *Phys. Rev. Lett.* **105**, 226102 (2010).

¹⁶H. Kim, J. Y. Zhang, S. Raghavan, and S. Stemmer, Direct Observation of Sr Vacancies in SrTiO₃ by Quantitative Scanning Transmission Electron Microscopy. *Phys. Rev. X* **6**, 041063 (2016).

¹⁷A. Karjalainen, V. Prozheeva, I. Makkonen, C. Guguschev, T. Markurt, M. Bickermann, and F. Tuomisto, Ti_{Sr} antisite: An abundant point defect in SrTiO₃. *J. Appl. Phys.* **127**, 245702 (2020).

¹⁸M. Siebenhofer, F. Baiutti, J. de Dios Sirvent, T. M. Huber, A. Viernstein, S. Smetaczek, C. Herzig, M. O. Liedke, M. Butterling, A. Wagner, E. Hirschmann, A. Limbeck, A. Tarancon, J. Fleig, and M. Kubicek, Exploring point defects and trap states in undoped SrTiO₃ single crystals. *J. Eur. Ceram. Soc.* **42**, 1510 (2022).

¹⁹S. Kobayashi, Y. Mizumukai, T. Ohnishi, N. Shibata, Y. Ikuhara, and T. Yamamoto, High Electron Mobility of Nb-Doped SrTiO₃ Films Stemming from Rod-Type Sr Vacancy Clusters. *ACS Nano* **9**, 10769 (2015).

²⁰P. C. Snijders, C. Sen, M. P. McConnell, Y. Z. Ma, A. F. May, A. Herklotz, A. T. Wong, and T. Z. Ward, Dynamic defect correlations dominate activated electronic transport in SrTiO₃. *Sci. Rep.* **6**, 30141 (2016).

²¹N. Osawa, R. Takahashi, and M. Lippmaa, Hole trap state analysis in SrTiO₃. *Appl. Phys. Lett.* **110**, 263902 (2017).

²²Y. Jin, F. Zhang, K. Zhou, C. H. Suen, X. Y. Zhou, and J.-Y. Dai, Oxygen vacancy and photoelectron enhanced flexoelectricity in perovskite SrTiO₃ crystal. *Appl. Phys. Lett.* **118**, 164101 (2021).

²³A. Stashans and L. Villamagua, Schottky defects in cubic lattice of SrTiO₃. *J. Phys. Chem. Solids* **70**, 417 (2009).

²⁴J. N. Baker, P. C. Bowes, J. S. Harris, and D. L. Irving, Mechanisms governing metal vacancy formation in BaTiO₃ and SrTiO₃. *J. Appl. Phys.* **124**, 114101 (2018).

²⁵A. Janotti, J. B. Varley, M. Choi, and C. G. Van de Walle, Vacancies and small polarons in SrTiO₃. *Phys. Rev. B* **90**, 085202 (2014).

²⁶R. A. Mackie, S. Singh, J. Laverock, S. B. Dugdale, and D. J. Keeble, Vacancy defect positron lifetimes in strontium titanate. *Phys. Rev. B* **79**, 014102 (2009).

²⁷X. Zheng, Y. Yang, C. Fang, and X. Liu, Stability of oxygen vacancies at metal/oxide interfaces. *Phys. Chem. Chem. Phys.* **25**, 19970 (2023).

²⁸B. Liu, V. R. Cooper, H. Xu, H. Xiao, Y. Zhang, and W. J. Weber, Composition dependent intrinsic defect structures in SrTiO₃. *Phys. Chem. Chem. Phys.* **16**, 15590 (2014).

²⁹J. B. Varley, A. Janotti, and C. G. Van de Walle, Hydrogenated vacancies and hidden hydrogen in SrTiO₃. *Phys. Rev. B* **89**, 075202 (2014).

³⁰J. E. Jaffe, R. M. Van Ginhoven, and W. Jiang, Interstitial and substitutional zirconium in SrTiO₃. *Comput. Mater. Sci.* **53**, 153 (2012).

³¹L. Triggiani, A. B. Muñoz-García, A. Agostiano, and M. Pavone, Promoting oxygen vacancy formation and p-type conductivity in SrTiO₃ via alkali metal doping: a first principles study. *Phys. Chem. Chem. Phys.* **18**, 28951 (2016).

³²F. Ellinger, M. Shafiq, I. Ahmad, M. Reticcioli, and C. Franchini, Small polaron formation on the Nb-doped SrTiO₃ (001) surface. *Phys. Rev. Mater.* **7**, 064602 (2023).

³³J. Crawford and P. Jacobs, Point Defect Energies for Strontium Titanate: A Pair-Potentials Study. *J. Solid State Chem.* **144**, 423 (1999).

- ³⁴F. El-Mellouhi, E. N. Brothers, M. J. Lucero, and G. E. Scuseria, Neutral defects in SrTiO₃ studied with screened hybrid density functional theory. *J. Phys. Condens. Matter* **25**, 135501 (2013).
- ³⁵C. Ricca, I. Timrov, M. Cococcioni, N. Marzari, and U. Aschauer, Self-consistent DFT+U+V study of oxygen vacancies in SrTiO₃. *Phys. Rev. Res.* **2**, 023313 (2020).
- ³⁶J. Souto-Casares, N. A. Spaldin, and C. Ederer, Oxygen vacancies in strontium titanate: A DFT+DMFT study. *Phys. Rev. Res.* **3**, 023027 (2021).
- ³⁷S. Winczewski, J. Dziedzic, T. Miruszewski, J. Rybicki, and M. Gazda, Properties of Oxygen Vacancy and Hydrogen Interstitial Defects in Strontium Titanate: DFT + U^{d,p} Calculations. *J. Phys. Chem. C* **126**, 18439 (2022).
- ³⁸J. N. Baker, P. C. Bowes, D. M. Long, A. Moballegh, J. S. Harris, E. C. Dickey, and D. L. Irving, Defect mechanisms of coloration in Fe-doped SrTiO₃ from first principles. *Appl. Phys. Lett.* **110**, 122903 (2017).
- ³⁹P. C. Bowes, J. N. Baker, J. S. Harris, B. D. Behrhorst, and D. L. Irving, Influence of impurities on the high temperature conductivity of SrTiO₃. *Appl. Phys. Lett.* **112**, 022902 (2018).
- ⁴⁰Z. Zhang and A. Janotti, Cause of Extremely Long-Lasting Room-Temperature Persistent Photoconductivity in SrTiO₃ and Related Materials. *Phys. Rev. Lett.* **125**, 126404 (2020).
- ⁴¹M. Choi, F. Oba, and I. Tanaka, Role of Ti antisite like defects in SrTiO₃. *Phys. Rev. Lett.* **103**, 185502 (2009).
- ⁴²O. O. Brovko and E. Tosatti, Controlling the magnetism of oxygen surface vacancies in SrTiO₃ through charging. *Phys. Rev. Mater.* **1**, 044405 (2017).
- ⁴³K. Klyukin and V. Alexandrov, Effect of intrinsic point defects on ferroelectric polarization behavior of SrTiO₃. *Phys. Rev. B* **95**, 035301 (2017).
- ⁴⁴P. Reunchan, N. Umezawa, A. Janotti, J. T-Thienprasert, and S. Limpijumnong, Energetics and optical properties of nitrogen impurities in SrTiO₃ from hybrid density-functional calculations. *Phys. Rev. B* **95**, 205204 (2017).
- ⁴⁵T. Xu, T. Shimada, M. Mori, G. Fujimoto, J. Wang, and T. Kitamura, Defect engineering for nontrivial multiferroic orders in SrTiO₃. *Phys. Rev. Mater.* **4**, 124405 (2020).
- ⁴⁶M. J. Akhtar, Z.-U.-N. Akhtar, R. A. Jackson, and C. R. A. Catlow, Computer Simulation Studies of Strontium Titanate. *J. Am. Ceram. Soc.* **78**, 421 (1995).
- ⁴⁷T. Tanaka, K. Matsunaga, Y. Ikuhara, and T. Yamamoto, First-principles study on structures and energetics of intrinsic vacancies in SrTiO₃. *Phys. Rev. B* **68**, 205213 (2003).
- ⁴⁸Y. Wu, P. C. Bowes, J. N. Baker, and D. L. Irving, Influence of space charge on the conductivity of nanocrystalline SrTiO₃. *J. Appl. Phys.* **128**, 014101 (2020).
- ⁴⁹S. R. K. Irea Mosquera-Lois, Aron Walsh, and David O. Scanlon, ShakeNBreak: Navigating the defect configurational landscape. *J. Open Source Softw.* **7**, 4817 (2022).
- ⁵⁰D. Lee, H. Wang, B. A. Noesges, T. J. Asel, J. Pan, J.-W. Lee, Q. Yan, L. J. Brillson, X. Wu, and C.-B. Eom, Identification of a functional point defect in SrTiO₃. *Phys. Rev. Mater.* **2**, 060403 (2018).
- ⁵¹K. Szot, W. Speier, R. Carius, U. Zastrow, and W. Beyer, Localized Metallic Conductivity and Self-Healing during Thermal Reduction of SrTiO₃. *Phys. Rev. Lett.* **88**, 075508 (2002).
- ⁵²C. Nath, C. Y. Chueh, Y. K. Kuo, and J. P. Singh, Thermoelectric properties of p-type SrTiO₃/graphene layers nanohybrids. *J. Appl. Phys.* **125**, 185101 (2019).
- ⁵³V. M. Poole, C. D. Corolewski, and M. D. McCluskey, P-type conductivity in annealed strontium titanate. *AIP Adv.* **5**, 127217 (2015).

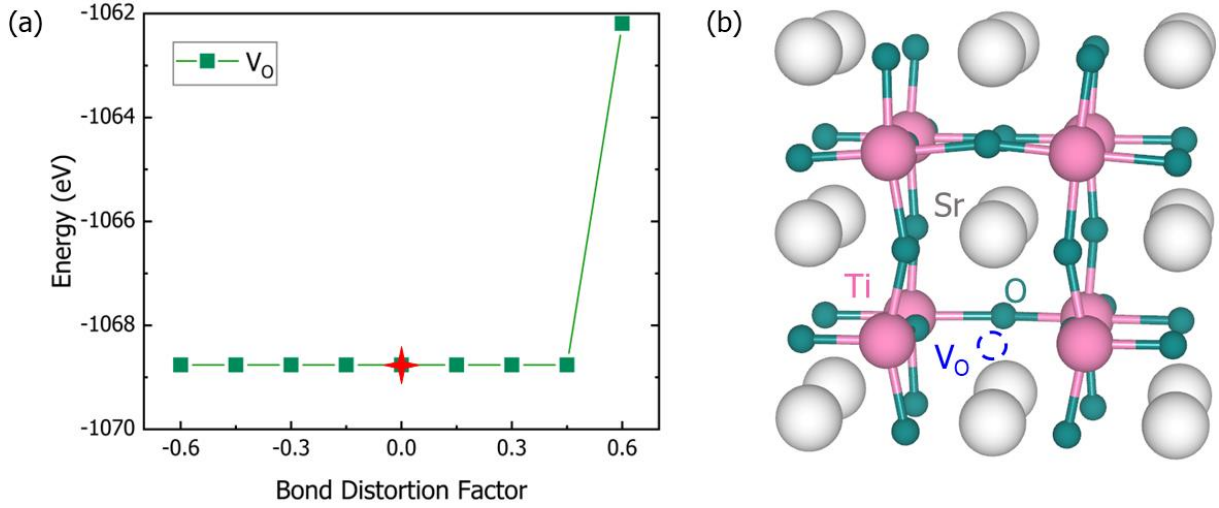


Figure 1. (a) Plot of final total energies of neutral V_O versus bond distortion factor. Negative distortion means the adjacent atoms move towards the defect and the positive distortion means the adjacent atoms move away from the defect. Zero means no distortion. All the distortions are relative to the equilibrium lattice position in the perfect cell; (b) The most stable structure of neutral V_O marked with a red star in (a).

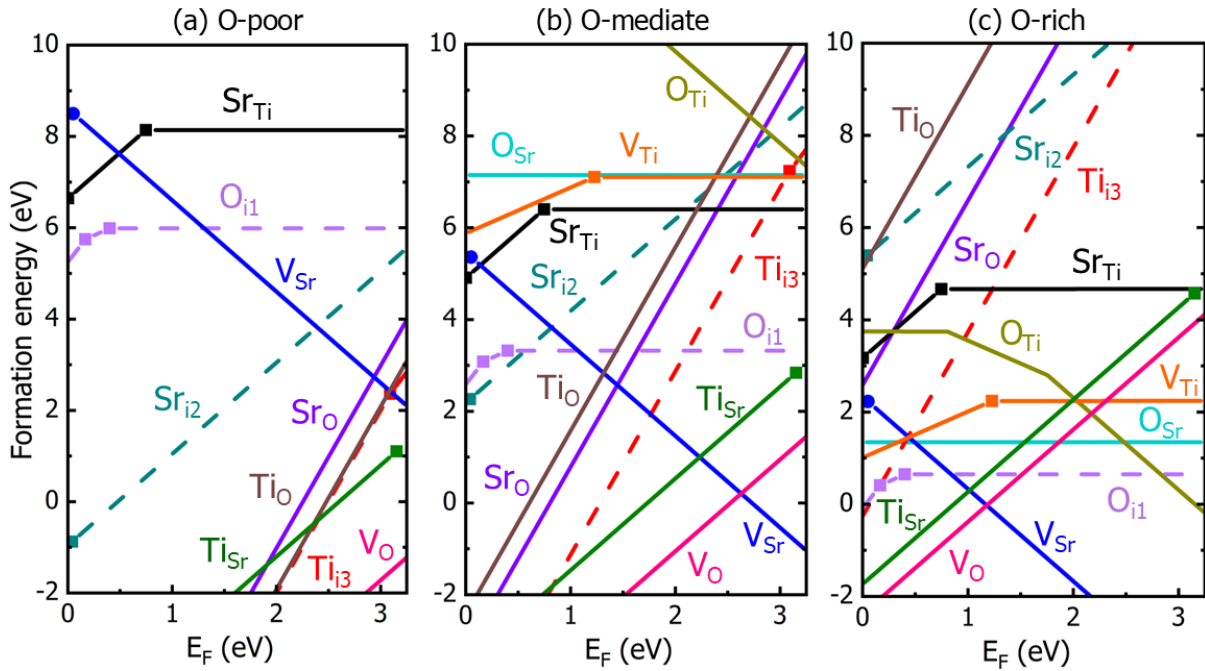


Figure 2. The calculated formation energies of intrinsic defects in STO as function of Fermi level (E_F) under: (a) O-poor condition ($\mu_O = -5.34$ eV, $\mu_{Sr} = -0.83$ eV, $\mu_{Ti} = -0.28$ eV); (b) O-mediate condition ($\mu_O = -2.67$ eV, $\mu_{Sr} = -3.97$ eV, $\mu_{Ti} = -5.15$ eV); (c) O-rich condition ($\mu_O = 0$ eV, $\mu_{Sr} = -7.10$ eV, $\mu_{Ti} = -10.02$ eV). Square and circle points represent the transition levels of donor and acceptor defects respectively as shown in Fig. 3(d).

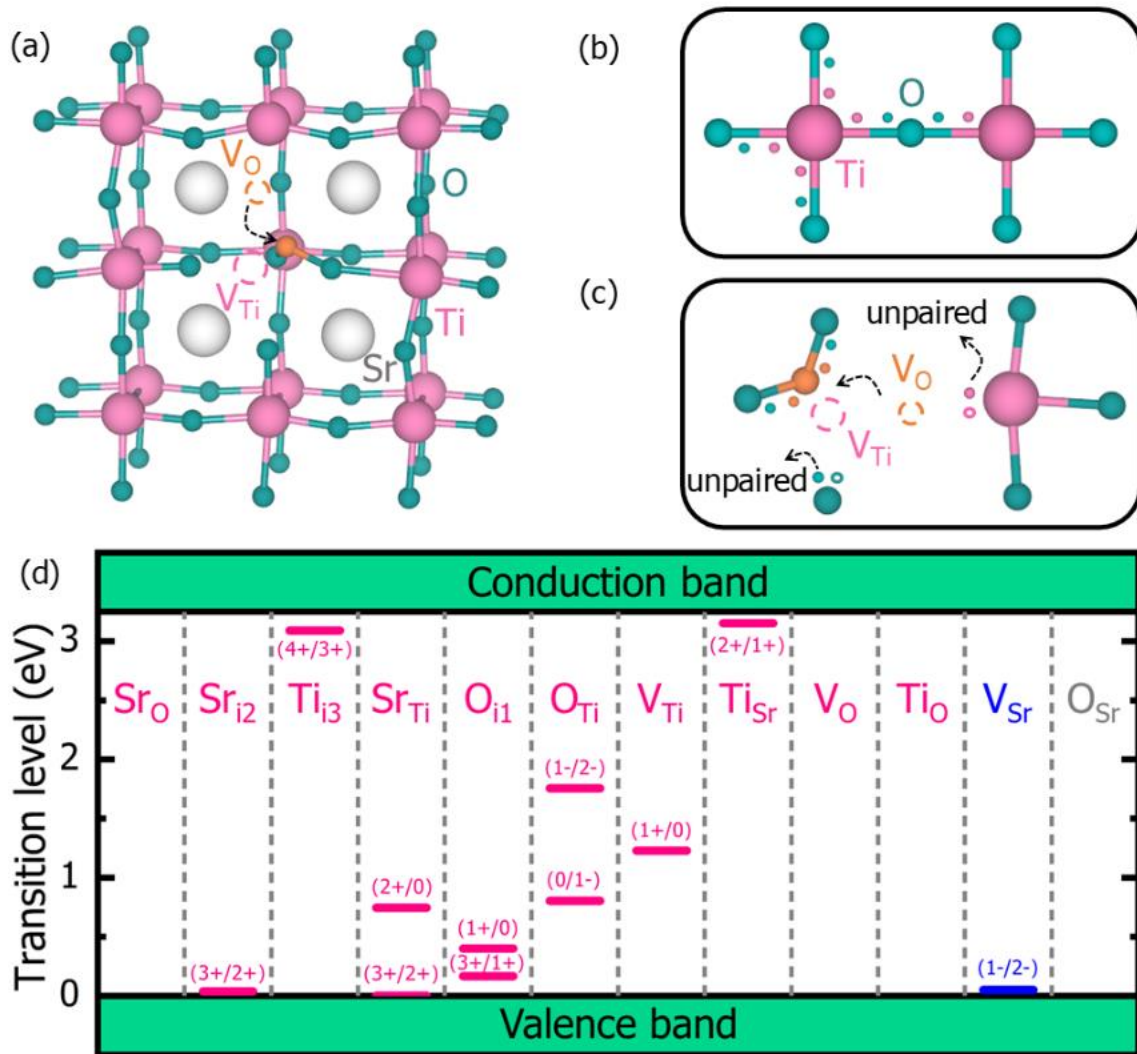


Figure 3. (a) The ground-state structure of neutral V_{Ti}; (b) and (c) are the bonding situation before and after forming neutral V_{Ti}; (d) The calculated transition levels of intrinsic defects in the band gap of STO.

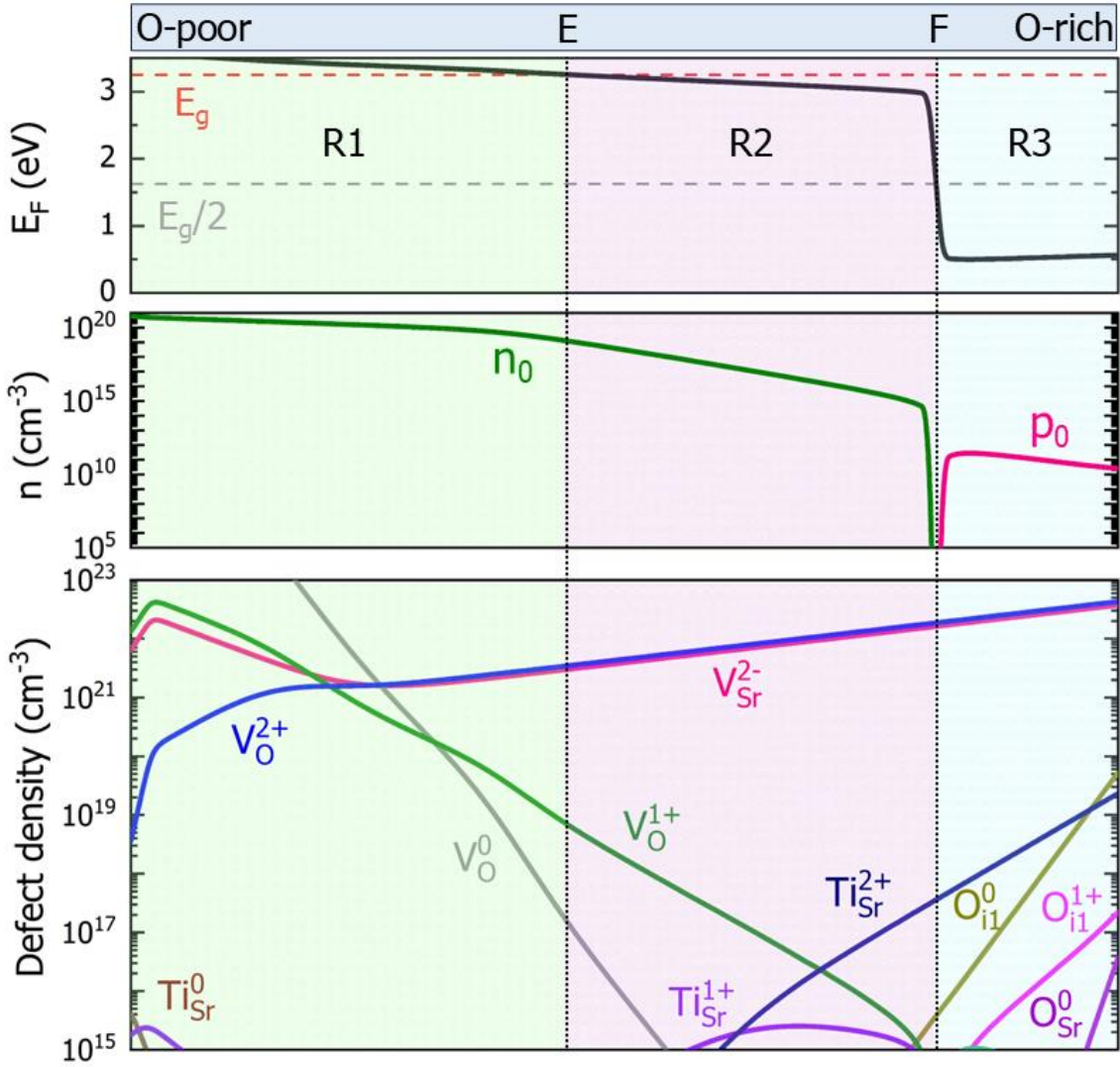


Figure 4. The calculated Fermi level (E_F), intrinsic carrier densities, and density of low-energy intrinsic defects in STO as function of O chemical potential (The specific chemical potential values of O-rich and O-poor are the same as that in Fig. 2). The middle of the band gap ($E_g/2$) is marked with a grey dashed line. The band gap (E_g) is marked with a red dashed line. E ($\mu_{\text{O}} = -2.99$ eV, $\mu_{\text{Sr}} = -3.59$ eV, $\mu_{\text{Ti}} = -4.56$ eV) is the transition point of conductivity from metallic to n-type. F ($\mu_{\text{O}} = -0.99$ eV, $\mu_{\text{Sr}} = -5.95$ eV, $\mu_{\text{Ti}} = -8.22$ eV) is the transition point of conductivity from n-type to p-type.